Nanosensor Location in the Human Circulatory System based on Electric Circuit Representation of Vessels

Jorge Torres Gómez
TU Berlin, Germany
torres-gomez@ccs-labs.org

Jorge Luis González Rios
University of Luxembourg,
Luxembourg
jorge.gonzalez@uni.lu

Falko Dressler
TU Berlin, Germany
dressler@ccs-labs.org

ABSTRACT

Nanotechnologies are advancing precision medicine applications, enhancing the detection and treatment of diseases. Traveling through the human vessels, nanosensors are envisioned to locally detect and actuate on targets very efficiently. In this area, modeling the behavior of traveling nanosensors in the human circulatory system helps developing new mechanisms for medical treatments. This paper explores the accurate modeling of the concentration level of the flowing nanosensors in vessels. We use a Markov chain formulation to predict the stationary distribution of them in the variety of vessel segments. To evaluate the transition probabilities of the Markov chain, we compute the blood flow based on the representation of vessels through electric circuit components. The resulting study reveals the dynamics of the movement of nanosensors in the blood flow yielding further details on their concentration level along vessels.

CCS CONCEPTS

• **Applied computing** → **Health informatics**; • **Hardware** → **Biology-related information processing**.

KEYWORDS

Human Circulatory System, Electric Circuit Simulator, Blood Pressure, Nanosensors, Nanosensor Flow

1 INTRODUCTION

In-body nanotechnology-focused research is today advancing applications for precision medicine. New technologies enhance healthcare supporting systems in this field while detecting and localizing anomalies in the human body [1]. Nanosensors are envisioned to travel through the human circulatory system (HCS), passively
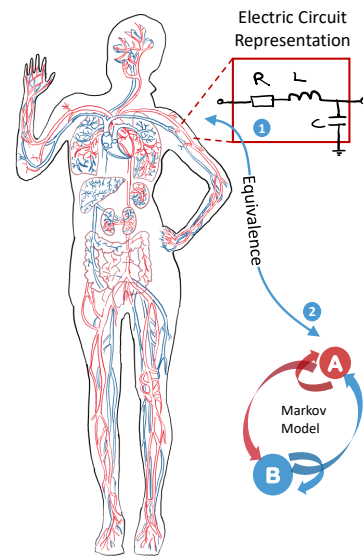
Figure 1: Electric-circuit representation in the arteries.

driven by the blood flow, and deliver the appropriate drug amount without affecting healthy capillaries around [3, 12]. In this endeavor, it is essential to assess location mechanisms for nanosensors in the vessels supporting the detection and treatment of diseases in specific target regions.

Driven by the blood flow, the exact location of nanosensors in vessels remains a challenging problem due to the non-predictable paths through arteries, capillaries, and veins. Jumps at bifurcations occur randomly resulting in a random process of the path trajectory of nanosensors in the vessels. Recent research addresses this issue through the use of anchor nodes and the exchange of reference coordinate location using wireless technology [11, 16], or calculating the distance to reference anchor nodes through hop-count metrics in the received messages [2, 21]. In a different approach, machine learning (ML) methods have been applied to leverage the traveling time of the nanosensor as an indicator of the path circuit in the body [19].

In this work, we follow on our previous methodology in [20], where the HCS is modeled through a Markov chain, and its transition matrix is evaluated relying on the electric circuit representation of the vessels. In this paper, for the electric circuit we implement a more complete design for the arteries from Noordergraaf et al. [13], providing a more accurate representation of the vessels, [1]. To evaluate the stationary distribution of nanosensors, we apply the

---

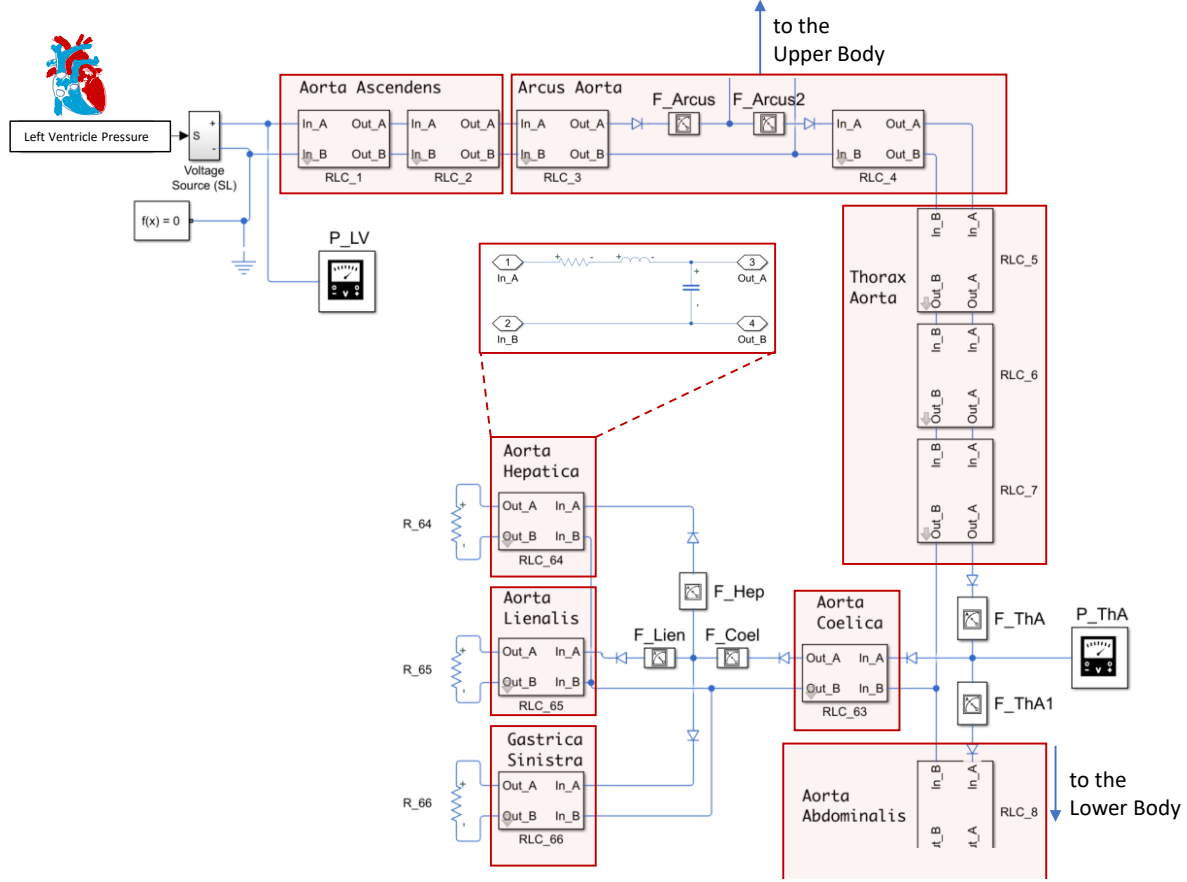[1]the design is publicly accessible in [18]

Figure 2: Electric circuit design of the human arteries according to [13]. The complete design is publicly available in [18]

tow-steps model in Fig. 1, in the first step, the flow in the vessel segments is computed directly from the currents in the electric circuit, in the second step the transition probabilities of the Markov chain are computed based on ratios of these flows. Based on the Markov chain representation, it is then possible to predict the stationary distribution of nanosensors along the vessels. This finds applicability to later assess their capabilities to detect and actuate on targets in the human vessels. Depending on their concentration level, they will be able to detect and actuate on a given target more or less impactful.

The electric circuit representation of the human vessels is conceived as 0-D models [4, 6, 13], providing the average flow and pressure (over the geometric coordinates of vessels), while significantly reducing computational resources. The time variable evolution of pressure and flow per vessel segment is directly given as voltages and currents provided by the circuit, respectively. In the literature, reported electric models for the HCS focus on both, the heart, where the systemic circulation is modeled with only one network, and the arteries, which are modelled as a cascade connection of L and Π two ports networks [4, 13, 15]. Since early work by Rideout [14], Snyder and Rideout [17], only a few works model the HCS as comprised of a more complete connection of arteries, capillaries, and veins. Although the work in [14] provides a more complete representation

of the HCS, the model lacks to implement the arms and the legs are analyzed as a single network; thereby providing fewer details.

This paper enhances our previously reported solution in [20] accounting for an electric circuit model comprising the head, arms, and legs as different circuit compartments. We describe the implementation of the electric circuit model in Simulink/Matlab (Section 2) and display the pressure curves along with the different artery segments. We also include additional stages in the Markov model (Section 3) based on the more detailed representation in the human arteries in accordance to Noordergraaf et al. [13]. Although this representation does not account for capillaries and veins, it provides the information needed to compute the transition matrix of the Markov model. Finally, we conclude the paper by illustrating the transition probabilities at bifurcations and the predicted concentration level of nanosensors per vessel segment (Section 4).

2 ELECTRIC CIRCUIT IMPLEMENTATION IN SIMULINK/MATLAB

We implement the electric circuit for the major arteries following the design provided by Noordergraaf et al. [13]. The circuit is conceived in Simulink/Matlab® using resistors, inductors, capacitors, and diodes from the Simscape library, (the design is publicly accessible in [18]). Fig. 2 illustrates the connection of blocks in the center
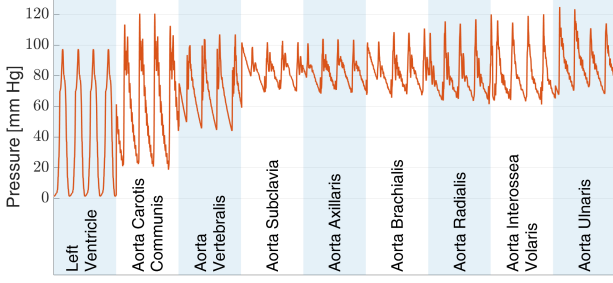
Figure 3: Blood pressure in the Head and the Arms.

Figure 4: Blood pressure in the Legs.

body for a variety of aorta segments. As represented in this figure, each aorta is implemented with the cascade connection of blocks denoted as RLC_x. Each of these blocks is implemented through an L-inverted topology, consisting in the series connection of a resistor and an inductor, and the shunt connection of a capacitor. The resistor, inductor, and capacitor, simulate the resistance to the blood flow, the inertia of the blood, and the compliance of the vessel, respectively, according to the specific segment in the aorta.

In this design, we also include diodes to guide the flow from arteries to the next segments in the same way the blood flows in the vessels. Due to the reactance of the capacitors and inductors, a flow back may be experienced due to the stored energy in these circuits, which is avoided with the addition of diodes. Finally, to reproduce the signal from the Heart we use the sequence generated for the left ventricle as given by the mathematical model in [9]. As for the complete design in [18], all the parameters are listed and the plots for pressure and flow can be also generated for each particular segment. In total, 128 blocks are implemented to complete the representation of the arteries in the head, center body, arms, and legs in accordance to Noordergraaf et al. [13].

Figures 3 and 4 provide the resulting pressure in the arms and the legs, those directly derived from the connected voltage meter. In accordance with the behavior of the blood pressure at different vessel segments [7], the largest oscillation is derived in the Left Ventricle (Heart) and its elongation is reduced in the arms and legs' arteries. We also remark the increased amplitude in the large arteries (e.g., Aorta Carotis) in comparison to the left ventricle as a typical behavior of the blood pressure in vessels.

The standard amplitude of pressure in the left ventricle is higher than reported in Fig. 3. Typically, it alternates around $120 \, \text{mm} \, \text{Hg}$ (*systolic*) and $80 \, \text{mm} \, \text{Hg}$ (*diastolic*) [7]. However, in our case, the lower amplitude of the oscillations is mostly driven by the model used for the heart. Future work will be conducted to implement an electric model for the Heart as well, providing a larger amplitude as the one we integrate is still a mathematical model [9].

3 MARKOV MODEL REPRESENTATION OF THE HUMAN CIRCULATORY SYSTEM

The path trajectory of the flowing nanosensors in the HCS can be modeled as a transition between stages, defined in one-to-one correspondence with the vessel segments. Assuming that transitions at bifurcations (to the next vessel segment in the arteries) happen randomly and independent of the previously visited vessel, the
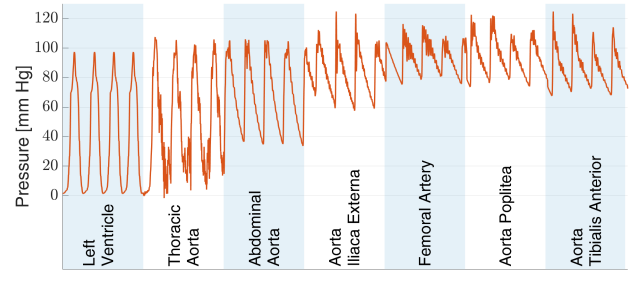
traveling path of the nanosensor can be modeled using a Markov chain approach [5].

Fig. 5 depicts the conceived stages for the Markov model following the variety of artery segments represented by the electric circuit design in Section 2. The veins in the Markov model are included when mirroring the corresponding artery (due to the symmetry of the human body), except for the head where the veins are reduced to two from four just for the seek of simplicity. In total 51 stages are conceived representing arteries, capillaries, and veins, as listed in Table 1. In contrast to our previous design [20, Fig. 5], the current one introduces additional stages accounting for the two arms and the two legs. A more complete representation is provided here due to the available representation of our circuit design.

The Markov model is completely defined by its transition matrix, denoted as $\Pi = \{p_{i,j}\}$, where $p_{i,j}$ are the transition probabilities. Besides, the stationary distribution of nanosensors can be directly evaluated when solving for ν in

$$\nu = \nu\Pi. \tag{1}$$

That is, the probability to find a nanosensor s on a given vessel segment k can be directly computed from the components of the vector ν as

$$P_{s,k} = v_k, \tag{2}$$

based on which we can estimate the concentration of nanosensors on a given vessel segment as $P_{s,k} \cdot N_s$, where N_s are the total of nanosensors flowing in the HCS.

The relation in Eq. (2) will ultimately depend on the transition probabilities between states of the Markov model. To compute those, we rely on the equivalent circuit representation of the Markov model comprised of nodes and oriented loops [10]. To illustrate, Fig. 6 depicts on the left side the representation of a Markov chain composed of 6 stages, out of which we can define three independent oriented loops, all of them intercepting through the nodes s_1, s_2, and s_3, as represented in the right side of the figure. According to [10], the equivalent representation is given by the unique relation between the weighted coefficients (ω_1, ω_2, and ω_3) along with the loops and the transition probabilities in the Markov model. For instance, if we want to evaluate the transition probability $p_{1,3}$ through this coefficients it yields

$$p_{1,3} = \frac{\omega_1}{\omega_1 + \omega_2 + \omega_3}, \tag{3}$$

as the ratio between the coefficient corresponding to the loop where the destination s_3 is located (ω_1 in this case), divided by the sum
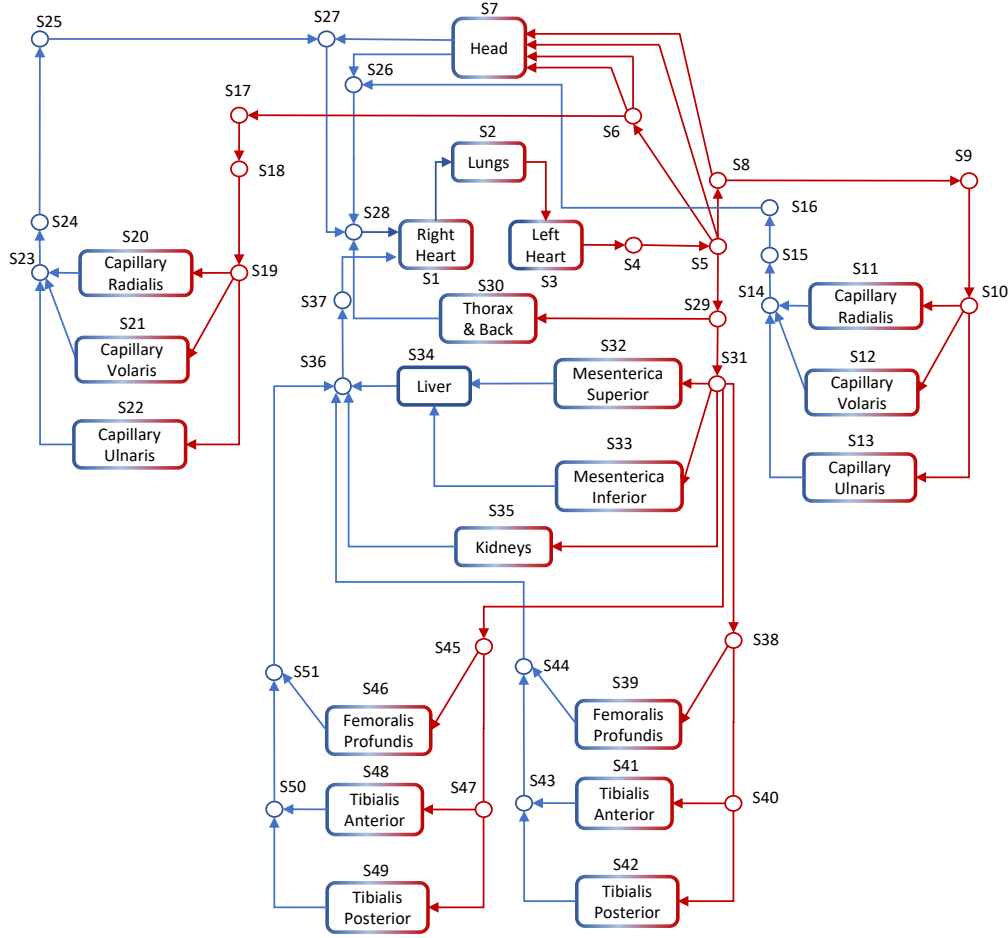
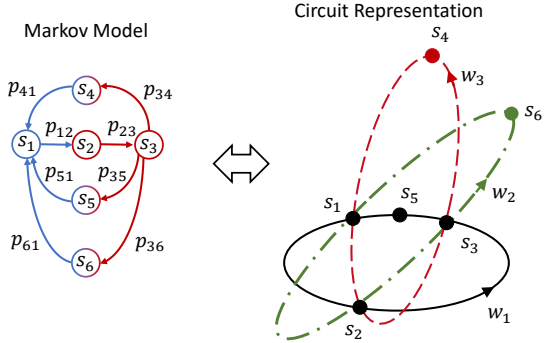**Figure 5: Markov model representation of the HCS.**

Figure 6: Circuit representation of a Markov chain.

of the coefficients concerning the loops intercepting the departing stage s_1 (the three loops in this case).

The way these coefficients are sketched (constant along the loop), together with the circuit topology of this representation, let us interpret this coefficient as mesh currents from the electric circuit that simulate the same HCS as the Markov model does [20]. That is, mesh currents are also constant along closed-loops [8], and they superpose in the same way the coefficient does in the

circuit representation of the Markov model. In this way, the transition probability in Eq. (3) can be computed considering the mesh currents in the electric circuit representation as

$$p_{1,3} = \frac{I_1}{I_1 + I_2 + I_3},\tag{4}$$

when interpreting the coefficients as mesh currents as I_k.

Extending this analysis to the original Markov model in Fig. 5, the transition probability from Arcus Aorta to Aorta Thoratica can be computed as the ratio of the output current from s_5 to s_{29}, to the input current to s_5, for instance. The same apply to the other bifurcations as well. Intuitively, this also matches the definition of probability as a ratio of successful events to the total of events. Looking at the corresponding ratio of flows as the total of particles moving to one branch in comparison to the total of particles at the bifurcation, let to interpret it as a metric of probability.

In this way, the electric circuit for the arteries in Section 2 let us compute the transition probabilities for the Markov model at the bifurcations. Besides, because transitions in the veins happen with a probability equal to 1, then the transition matrix of the Markov model can be fully determined in this way. We remark that according to the model in Fig. 5, there are two output veins
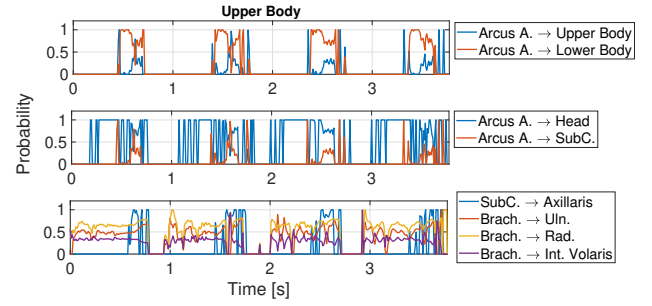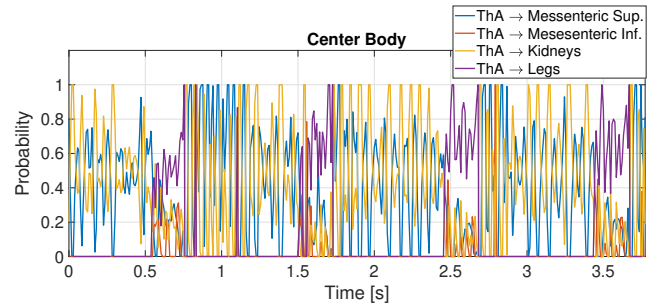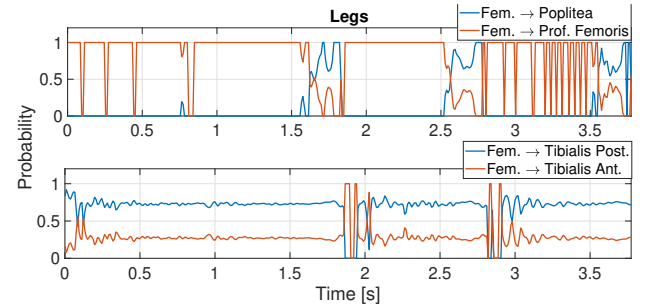
Table 1: Association between stages and vessel segments.

Markov States	Vessel Segment
S1	Right Heart
S2	Lungs
S3	Left Heart
S4	A. Ascendens
S5	Arcus Aorta
S6	A. Anonyma
S7	Head
S8 (S17)	A. Subclavia s. (d)
S9 (S18)	A. Axillaris s. (d.)
S10 (S19)	A.Brachialis s. (d.)
S11 (S20)	A. Radialis s. (d.)
S12 (S21)	A. Interossea Volaris s. (d.)
S13 (S22)	A. Ulnaris s. (d.)
S14 (S23)	V. Brachialis s. (d.)
S15 (S24)	V. Axillaris s. (d.)
S16 (S25)	V. Subclavia s. (d.)
S26 (S27)	Jugular Vein s. (d.)
S28	Superior Vena Cava
S29	Thoratica Aorta
S30	Thorax and Back
S31	Abdominal Aorta
S32	Mesenterica Superior
S33	Mesenterica Inferior
S34	Liver
S35	Kidneys
S36	Abdominal Vein
S37	Inferior Vena Cava
S38 (S45)	A. Iliaca Communis and Externa s. (d.)
S39 (S46)	A. Femoralis Profundis s. (d.)
S40 (47)	A. Poplitea s. (d.)
S41 (S48)	A. Tibialis Anterior s. (d.)
S42 (S49)	A. Tibialis Posterior s. (d.)
S43 (S50)	V. Poplitea s. (d.)
S44 (S51)	V. Iliaca Communis and Externa s. (d.)

represented in the Head towards the stages S26 and S27. For the sake of simplicity here we assume equal probability, although a more accurate model can be obtained according to the ratio of flows from both veins (Carotid and Vertebralis in this case).

4 RESULTS

In this Section, we illustrate results concerning the obtaining of the transition matrix for the Markov model, and its use to predict the

Figure 7: Transition probabilities in the upper body.

Figure 8: Transition probabilities in the center body.

Figure 9: Transition probabilities in the lower body.

concentration level of nanosensors along the vessels. Figures 7 to 9 show the transition probabilities versus time at main bifurcations in the upper, center and lower bodies, respectively. We compute the transition probabilities directly evaluating the ratio of corresponding current flows, as described in Eq. (4), where the flow is measured by current meters located in the design (e.g., the blocks F_ThA and F_ThA1 in Fig. 2).

As shown in Fig. 7, most of the time transitions are favored in the direction of the lower body, than the upper body. That is, from the left ventricle (S4) a larger flow follows to the lower body through Arcus Aorta (S5), which is in correspondence to the larger cross-sectional area of the Thorax Aorta (S31). This result also matches our previous calculation of transition probabilities in [20, Fig. 7] using the electric circuit design from [14, 17], where the larger probability is also in the direction of the lower body. Besides, according to the plots in Fig. 7, most of the time nanosensors will be traveling to the head (through Carotis and Vertebralis) than to the arms in the direction of the Subclavia and the Aorta Axillaris.
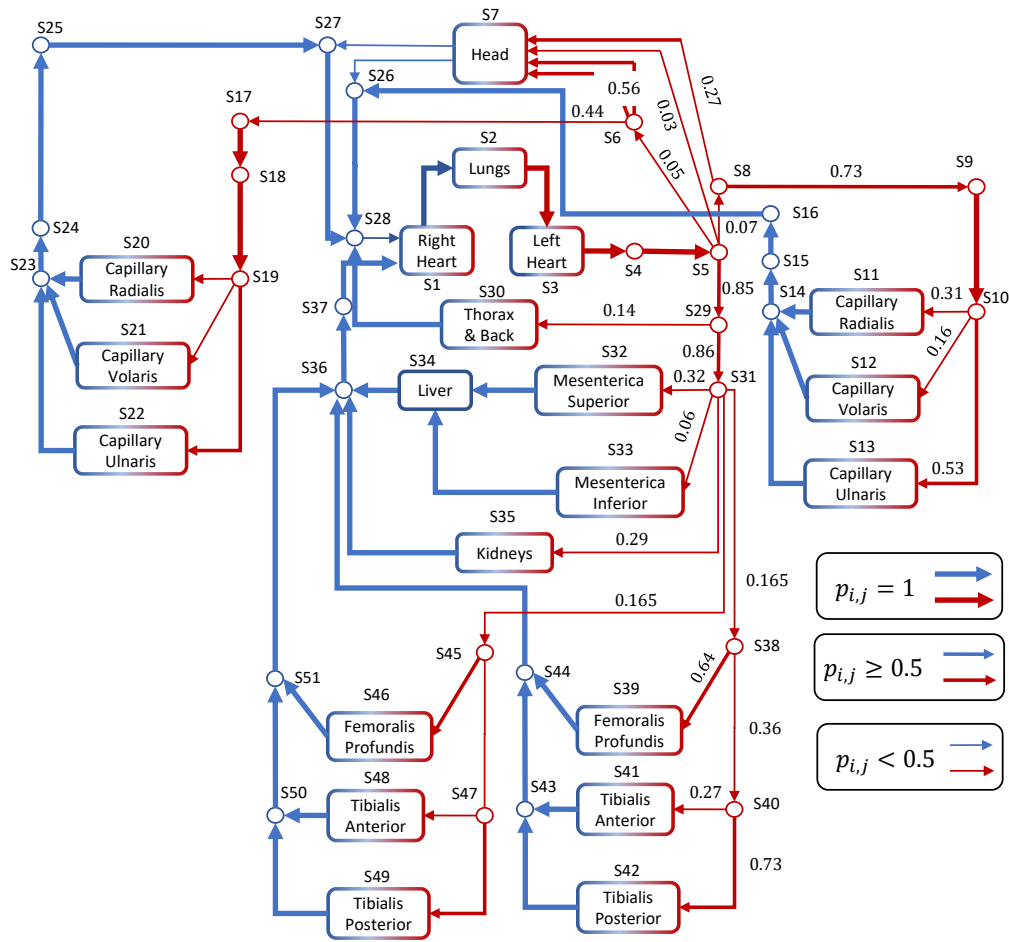
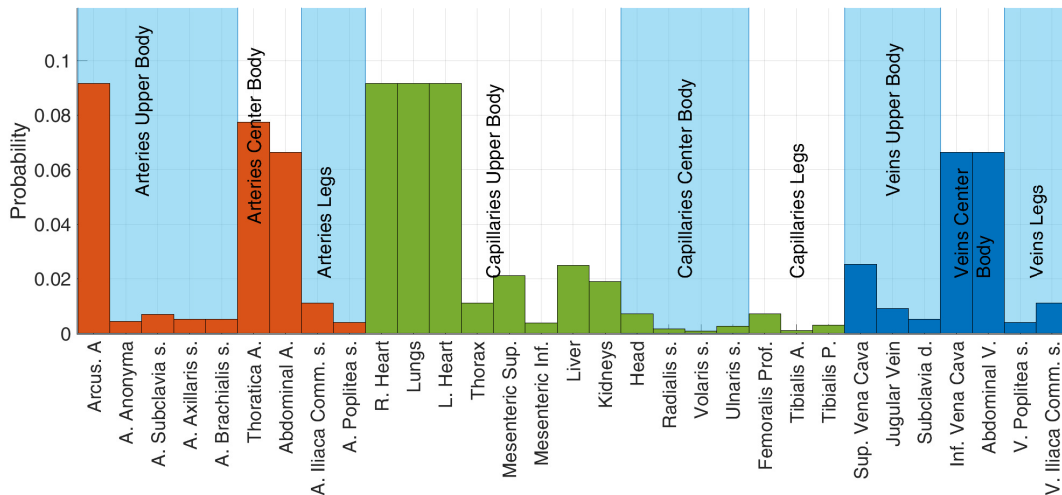Figure 10: Transition probabilities represented by the width of the edges.

Figure 11: Distribution of nanosensors in the HCS.

In the center body (cf. Fig. 8), most of the time transitions happen to the Kidneys and to the Messenterica Superior. Fewer transitions

happens to the Messenteric Inferior or the legs with time. Besides,

accounting for the lower body (cf. Fig. 9), we remark the less variability of the transition probabilities with time in the legs. This is a consequence of the less variability of the pressure as these body regions are more distant from the heart. According to these plots, most of the time nanosensors will be traveling through the Profundis Femoris in the legs than to the Poplitea or the Posterior and Anterior Tibialis.

Using these transition probabilities at the bifurcations, we complete the transition matrix of the Markov model. To do so, we average these transition probabilities over time and set equal to one the transition probabilities in the veins. In the case of the output veins from the head, we assume equal probability to travel through the Vertebralis or the Carotis for the seek of simplicity, although more accurate values can be derived based on the flows on each vessel. The resulting procedure is illustrated in Fig. 10, where the width of the arrows is used to illustrate where the averaged transition probabilities are one, higher, or less than 0.5. As exhibited in this graph, the larger transition probabilities are obtained at bifurcations for those paths addressing the head, the center body, the Femoris Profundis, and the Tibialis Posterior.

Using these average transition probabilities, then the stationary distribution can be derived using Eq. (2) after solving Eq. (1). The results are plotted in Fig. 11, where the length of the bars indicates the probability to locate a given nanosensor along with the vessel's segments. As exhibited in this figure, the largest probability is obtained at the Arcus and Thoratica Aorta, the Heart, the Lungs, and the Superior Vena Cava. In this case, the probability is around 0.1 which is close to the probability derived in our previous work in [20, Fig. 9]. However, in contrast to our previous work, in this case, the Superior Vena Cava exhibits a larger probability than the Inferior Vena Cava. This is a consequence of the inclusion of the two arms and the connection of the Thorax capillaries to the Superior Vena Cava. Finally, according to these bars, the less probability to find a nanosensor is given in the Mesenteric Inferior and the capillaries in the arms and legs.

5 CONCLUSION

This work underlines an effective methodology to predict the concentration of nanosensors traveling in the blood flow. Relying on the Markov model representation of the human circulatory system, the methodology employs a low complex electric circuit to evaluate the transition probabilities. Results exhibit a good correspondence to our previous work and the expected distribution of nanosensors along with the vessel segments. Future work will be conducted to include an electric circuit design for the heart and the lungs. Besides, we will include additional vessel segments for a more detailed representation of the human circulatory system.

REFERENCES

[1] Ian F. Akyildiz, Massimiliano Pierobon, and Sasitharan Balasubramaniam. 2019. Moving forward with molecular communication: from theory to human health applications [point of view]. *Proc. IEEE* 107, 5 (May 2019), 858–865. https://doi.org/10.1109/jproc.2019.2913890

[2] Florian Büther, Immo Traupe, and Sebastian Ebers. 2018. Hop Count Routing: A Routing Algorithm for Resource Constrained, Identity-Free Medical Nanonetworks. In *5th ACM International Conference on Nanoscale Computing and Communication (NANOCOM 2018)*. ACM, Reykjavík, Iceland. https://doi.org/10.1145/3233188.3233193

[3] Uche A. K. Chude-Okonkwo, Reza Malekian, B. T. Maharaj, and Athanasios V. Vasilakos. 2017. Molecular Communication and Nanonetwork for Targeted Drug Delivery: A Survey. *IEEE Communications Surveys & Tutorials* 19, 4 (2017), 3046–3096. https://doi.org/10.1109/comst.2017.2705740

[4] Luca Formaggia, Alfio Quarteroni, and Alessandro Veneziani. 2006. The circulatory system: from case studies to mathematical modeling. In *Complex Systems in Biomedicine*, Alfio Quarteroni, Luca Formaggia, and Alessandro Veneziani (Eds.). Springer Milan, Milano, Italy, 243–287. https://doi.org/10.1007/88-470-0396-2_7

[5] Constantine Gatsonis, James S. Hodges, Robert E. Kaas, and Nozer D. Singpurwalla. 2012. *Case Studies in Bayesian Statistics*. Vol. II. Springer Science & Business Media.

[6] Raheem Gul. 2016. *Mathematical Modeling and Sensitivity Analysis of Lumped-Parameter Model of the Human Cardiovascular System.* PhD Thesis. Freien Universität Berlin. Advisor(s) Schütte, Christof and Bernhard, Stefan.

[7] Arthur C. Guyton and Michael. E. Hall. 2015. *Guyton and Hall Textbook of Medical Physiology* (14 ed.). Elsevier.

[8] William Hayt, Jack Kemmerly, Jamie Phillips, and Steven Durbin. 2019. *Engineering Circuit Analysis* (9 ed.). McGraw-Hill Education, New York City, NY.

[9] Zhe Hu. 2001. HSP. https://de.mathworks.com/matlabcentral/fileexchange/818-hsp

[10] Sophia L. Kalpazidou. 2006. Genesis of Markov Chains by Circuits: The Circuit Chains. In *Cycle Representations of Markov Processes* (2 ed.), B. Rozovskii (Ed.). Vol. 28. Springer, 17–28.

[11] Filip Lemic, Sergi Abadal, Eduard Alarcón, and Jeroen Famaey. 2021. *Toward Location-aware In-body Terahertz Nanonetworks with Energy Harvesting.* cs.ET 2101.01952. arXiv.

[12] Tadashi Nakano, Michael J. Moore, Fang Wei, Athanasios V. Vasilakos, and Jianwei Shuai. 2012. Molecular Communication and Networking: Opportunities and Challenges. *IEEE Transactions on NanoBioscience* 11, 2 (6 2012), 135–148. https://doi.org/10.1109/TNB.2012.2191570

[13] Abraham Noordergraaf, Pieter D. Verdouw, and Herman B.K. Boom. 1963. The use of an analog computer in a circulation model. *Progress in Cardiovascular Diseases* 5, 5 (March 1963), 419–439. https://doi.org/10.1016/s0033-0620(63)80009-2

[14] Vincent C. Rideout. 1991. *Mathematical and Computer Modeling of Physiological Systems.* Prentice Hall, Upper Saddle River, NJ.

[15] Yubing Shi, Patricia Lawford, and Rodney Hose. 2011. Review of Zero-D and 1-D Models of Blood Flow in the Cardiovascular System. *BioMedical Engineering OnLine* 10, 1 (2011), 33. https://doi.org/10.1186/1475-925x-10-33

[16] Jennifer Simonjan, Bige Deniz Unluturk, and Ian F. Akyildiz. 2021. In-body Bionanosensor Localization for Anomaly Detection via Inertial Positioning and THz Backscattering Communication. *IEEE Transactions on NanoBioscience* (2021), 1–1. https://doi.org/10.1109/tnb.2021.3123972

[17] M. F. Snyder and V. C. Rideout. 1969. Computer Simulation Studies of the Venous Circulation. *IEEE Transactions on Biomedical Engineering* BME-16, 4 (Oct. 1969), 325–334. https://doi.org/10.1109/tbme.1969.4502663

[18] Jorge Torres Gómez. 2022. Electric Circuit representation of the Human Arteries. https://www.mathworks.com/matlabcentral/fileexchange/109935-electric-circuit-representation-of-the-human-arteries

[19] Jorge Torres Gómez, Anke Kuestner, Ketki Pitke, Jennifer Simonjan, Bige Deniz Unluturk, and Falko Dressler. 2021. A Machine Learning Approach for Abnormality Detection in Blood Vessels via Mobile Nanosensors. In *19th ACM Conference on Embedded Networked Sensor Systems (SenSys 2021), 2nd ACM International Workshop on Nanoscale Computing, Communication, and Applications (NanoCoCoA 2021)*. ACM, Coimbra, Portugal, 596–602. https://doi.org/10.1145/3485730.3494037

[20] Jorge Torres Gómez, Regine Wendt, Anke Kuestner, Ketki Pitke, Lukas Stratmann, and Falko Dressler. 2021. Markov Model for the Flow of Nanobots in the Human Circulatory System. In *8th ACM International Conference on Nanoscale Computing and Communication (NANOCOM 2021)*. ACM, Virtual Conference, 5:1–5:7. https://doi.org/10.1145/3477206.3477477

[21] Lina Zhou, Guangjie Han, and Li Liu. 2017. Pulse-Based Distance Accumulation Localization Algorithm for Wireless Nanosensor Networks. *IEEE Access* 5 (2017), 14380–14390. https://doi.org/10.1109/access.2017.2732351